# Engineering of fast population transfer in three-level systems

Xi Chen[1,2] and J. G. Muga[1,2]

[1]*Departamento de Química-Física, UPV-EHU, Apdo 644, 48080 Bilbao, Spain*
[2]*Department of Physics, Shanghai University, 200444 Shanghai, People's Republic of China*

We design, by invariant-based inverse engineering, resonant laser pulses to perform fast population transfers in three-level systems. The laser intensities to improve the fidelity or to achieve a perfect transfer are examined for different protocols. They can be reduced by populating the intermediate state and by multimode driving.

PACS number(s): 32.80.Xx, 32.80.Qk, 33.80.Be

## I. INTRODUCTION

Controlling the internal state preparation and the system dynamics by electromagnetic pulses is crucial in atomic and molecular physics for applications such as metrology, interferometry, quantum information processing, or driving of chemical reactions [1–5]. In two- or three-level systems, resonant pulses, rapid adiabatic passage (RAP), stimulated Raman adiabatic passage (STIRAP), and their variants have been widely used to perform population transfers [2–4]. Resonant pulses may be fast, but are highly sensitive to the deviations of pulse areas and exact resonances, whereas the adiabatic passage techniques are robust versus variations in experimental parameters but slow. To combine the advantages of resonant pulses and adiabatic techniques and achieve fast and high-fidelity quantum state control, some alternative approaches, like composite pulses [6–8] and optimal control theory [9–13], have been proposed. Several recent works on "shortcuts to adiabaticity" have been also devoted to internal state population transfer [14–22]. The shortcut techniques include counterdiabatic control protocols [14] or, equivalently, transitionless quantum driving [15–17], "fast-forward" scaling [23], and inverse engineering based on Lewis-Riesenfeld invariants [24,25]. These methods are in fact strongly related, and even potentially equivalent [18,26]. However, they provide in general different shortcuts [18,21].

In this paper, we apply invariant-based engineering to realize fast and robust population transfers in three-level systems. This method has been applied in trap expansions [24,25,27–30], rotations [31], atom transport [32–34], mechanical oscillators [35], or many-body systems [36,37]. In a three-level system as the one depicted in Fig. 1, STIRAP allows one to transfer the population adiabatically from the initial state $|1\rangle$ to the target state $|3\rangle$. To speed up the process, a fast-driving counterdiabatic field connecting levels $|1\rangle$ and $|3\rangle$ may be used [16,38]. In general, though, it implies a weak magnetic dipole transition, which limits the ability of the counterdiabatic field to shorten the times [16,38]. Invariant-based engineering solves this by providing alternative shortcuts that do not couple directly levels $|1\rangle$ and $|3\rangle$.

## II. INVARIANT DYNAMICS

The Hamiltonian for STIRAP within the rotating wave approximation (RWA) reads

$$H_0(t) = \frac{\hbar}{2} \begin{pmatrix} 0 & \Omega_p(t) & 0 \\ \Omega_p(t) & 2\Delta_p & \Omega_s(t) \\ 0 & \Omega_s(t) & 2\Delta_3 \end{pmatrix}, \tag{1}$$

where, as shown in Fig. 1, the Rabi frequencies $\Omega_s(t)$ and $\Omega_p(t)$ describe the interactions with the pump and Stokes fields, and the detunings from resonance are defined as $\Delta_p = (E_2 - E_1)/\hbar - \omega_p$, $\Delta_s = (E_2 - E_3)/\hbar - \omega_s$, and $\Delta_3 = \Delta_s - \Delta_p$, where $\omega_s$ and $\omega_p$ are the laser (angular) frequencies, and $E_j$, $j = 1,2,3$, the bare-basis-state energies.

We consider the so-called "one-photon resonance" case, $\Delta_p = \Delta_3 = 0$, to simplify the Hamiltonian as

$$H(t) = \frac{\hbar}{2} \begin{pmatrix} 0 & \Omega_p(t) & 0 \\ \Omega_p(t) & 0 & \Omega_s(t) \\ 0 & \Omega_s(t) & 0 \end{pmatrix}. \tag{2}$$

The corresponding instantaneous eigenstates $|n\rangle$, with eigenvalues $E_0 = 0$ and $E_\pm = \pm\hbar\Omega/2$, with $\Omega = \sqrt{\Omega_p^2 + \Omega_s^2}$, are

$$|n_0(t)\rangle = \begin{pmatrix} \cos\theta \\ 0 \\ -\sin\theta \end{pmatrix}, \quad |n_\pm(t)\rangle = \frac{1}{\sqrt{2}} \begin{pmatrix} \sin\theta \\ \pm 1 \\ \cos\theta \end{pmatrix}, \tag{3}$$

where $\tan\theta = \Omega_p/\Omega_s$. When the adiabatic condition, $|\dot\theta| \ll |\Omega|$, is satisfied, perfect population transfer from the ground state $|1\rangle$ to the excited state $|3\rangle$ can be achieved adiabatically along the dark state $|n_0\rangle$, using the counterintuitive pulse order (Stokes before pump). We shall instead speed up the population transfer by using a dynamical invariant. To construct it, the Hamiltonian in Eq. (2) can be rewritten as [39]

$$H(t) = \frac{\hbar}{2}[\Omega_p(t)\hat{K}_1 + \Omega_s(t)\hat{K}_2], \tag{4}$$

where $\hat{K}_1$, $\hat{K}_2$, and $\hat{K}_3$ are angular-momentum operators for spin 1 [39],

$$\hat{K}_1 = \begin{pmatrix} 0 & 1 & 0 \\ 1 & 0 & 0 \\ 0 & 0 & 0 \end{pmatrix}, \quad \hat{K}_2 = \begin{pmatrix} 0 & 0 & 0 \\ 0 & 0 & 1 \\ 0 & 1 & 0 \end{pmatrix}, \quad \hat{K}_3 = \begin{pmatrix} 0 & 0 & -i \\ 0 & 0 & 0 \\ i & 0 & 0 \end{pmatrix},$$

that satisfy the commutation relations

$$[\hat{K}_1, \hat{K}_2] = i\hat{K}_3, \ [\hat{K}_2, \hat{K}_3] = i\hat{K}_1, \ [\hat{K}_3, \hat{K}_1] = i\hat{K}_2. \tag{5}$$

The Hamiltonian (2) possesses SU(2) dynamical symmetry, and an invariant $I(t)$, such that $dI/dt \equiv \partial I(t)/\partial t + (1/i\hbar)[I(t), H(t)] = 0$, is given by [18,40]

$$I(t) = \frac{\hbar}{2}\Omega_0(\cos\gamma\sin\beta\,\hat{K}_1 + \cos\gamma\cos\beta\,\hat{K}_2 + \sin\gamma\,\hat{K}_3)$$

$$= \frac{\hbar}{2}\Omega_0 \begin{pmatrix} 0 & \cos\gamma\sin\beta & -i\sin\gamma \\ \cos\gamma\sin\beta & 0 & \cos\gamma\cos\beta \\ i\sin\gamma & \cos\gamma\cos\beta & 0 \end{pmatrix}, \tag{6}$$

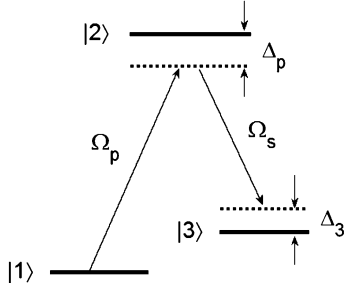FIG. 1. Level scheme of STIRAP for a $\Lambda$ level configuration. $\Omega_p$ and $\Omega_s$ are the Rabi frequencies for the interactions with the pump and Stokes fields, respectively, and $\Delta_p$ and $\Delta_3$ are the detunings from the resonances.

where $\Omega_0$ is an arbitrary constant with units of frequency to keep $I(t)$ with dimensions of energy, and the time-dependent auxiliary parameters $\gamma$ and $\beta$ satisfy the equations

$$\dot{\gamma} = \tfrac{1}{2}(\Omega_p \cos \beta - \Omega_s \sin \beta), \tag{7}$$

$$\dot{\beta} = \tfrac{1}{2} \tan \gamma (\Omega_s \cos \beta + \Omega_p \sin \beta), \tag{8}$$

where the dot represents a time derivative. The eigenstates of the invariant $I(t)$, which satisfy $I(t)|\phi_n(t)\rangle = \lambda_n|\phi_n(t)\rangle$, (we use the labels $n = 0, \pm$) are

$$|\phi_0(t)\rangle = \begin{pmatrix} \cos \gamma \cos \beta \\ -i \sin \gamma \\ -\cos \gamma \sin \beta \end{pmatrix} \tag{9}$$

and

$$|\phi_\pm(t)\rangle = \frac{1}{\sqrt{2}} \begin{pmatrix} \sin \gamma \cos \beta \pm i \sin \beta \\ i \cos \gamma \\ -\sin \gamma \sin \beta \pm i \cos \beta \end{pmatrix}, \tag{10}$$

corresponding to the eigenvalues $\lambda_0 = 0$ and $\lambda_\pm = \pm 1$. According to Lewis-Riesenfeld theory [41], the solution of the Schrödinger equation, $i\hbar \partial_t \Psi = H\Psi$, is a superposition of orthonormal "dynamical modes," $\Psi(t) = \sum_n C_n e^{i\alpha_n}|\phi_n(t)\rangle$ [41], where $C_n$ is a time-independent amplitude and $\alpha_n$ is the Lewis-Riesenfeld phase,

$$\alpha_n(t) = \frac{1}{\hbar} \int_0^t \langle \phi_n(t')|i\hbar \frac{\partial}{\partial t'} - H(t')|\phi_n(t')\rangle dt'. \tag{11}$$

In our case $\alpha_0 = 0$, whereas

$$\alpha_\pm = \mp \int_0^t \left[ \dot{\beta} \sin \gamma + \frac{1}{2} \left( \Omega_p \sin \beta + \Omega_s \cos \beta \right) \cos \gamma \right] dt'.$$

## III. INVERSE ENGINEERING AND FAST POPULATION TRANSFER

To design $\Omega_s$ and $\Omega_p$ we write them first, using Eqs. (7) and (8), in terms of $\gamma$ and $\beta$,

$$\Omega_s = 2(\dot{\beta} \cot \gamma \cos \beta - \dot{\gamma} \sin \beta), \tag{12}$$

$$\Omega_p = 2(\dot{\beta} \cot \gamma \sin \beta + \dot{\gamma} \cos \beta). \tag{13}$$

Once the appropriate boundary conditions for $\gamma$ and $\beta$ are fixed, we interpolate them with some ansatz, for example,

a polynomial or some other function with enough free parameters, so that $\Omega_s$ and $\Omega_p$ are determined.

Our Hamiltonian $H(t)$, Eq. (2), should drive the initial state $|1\rangle$ to the target state $|3\rangle$, up to a phase factor, along the invariant eigenstate $|\phi_0(t)\rangle$ in a given time $t_f$. We therefore write down the boundary conditions for $\gamma$ and $\beta$, based on Eq. (9),

$$\gamma(0) = 0, \gamma(t_f) = 0, \tag{14}$$

$$\beta(0) = 0, \beta(t_f) = \pi/2. \tag{15}$$

In general, $H(t)$ does not commute with the invariant $I(t)$, and they do not have common eigenstates. To achieve fast adiabaticlike passage (i.e., not really adiabatic all along but leading to the same final populations), one may impose boundary conditions to satisfy $[H(0), I(0)] = 0$ and $[H(t_f), I(t_f)] = 0$, which give $\Omega_p(0) = 0$ and $\Omega_s(t_f) = 0$. Using Eqs. (12)–(15) this implies the additional boundary conditions

$$\dot{\gamma}(0) = 0, \dot{\gamma}(t_f) = 0. \tag{16}$$

The set of conditions in Eqs. (14)–(16) guarantees fast adiabaticlike population transfer. Now we are ready to apply inverse engineering by means of different protocols. The examples discussed below are not exhaustive.

*Protocol 1.* In the first protocol, we set the boundary conditions for $\gamma$ and $\beta$ as follows:

$$\gamma(0) = \epsilon, \dot{\gamma}(0) = 0, \gamma(t_f) = \epsilon, \dot{\gamma}(t_f) = 0, \tag{17}$$

$$\beta(0) = 0, \beta(t_f) = \pi/2. \tag{18}$$

In contrast to Eq. (14) we have set a small value $\epsilon$ for $\gamma(0)$ and $\gamma(t_f)$, as an exact zero value implies infinite Rabi frequencies according to Eqs. (12) and (13). Consistent with these boundary conditions, we can simply choose

$$\gamma(t) = \epsilon, \beta(t) = \pi t / 2t_f, \tag{19}$$

which provides

$$\Omega_s(t) = (\pi/t_f) \cot \epsilon \cos (\pi t / 2t_f), \tag{20}$$

$$\Omega_p(t) = (\pi/t_f) \cot \epsilon \sin (\pi t / 2t_f). \tag{21}$$

Figure 2 shows the time evolution of Rabi frequencies and corresponding population transfer for $\Psi(t)$ with initial and final states $|\phi_0(0)\rangle$ and $|\phi_0(t_f)\rangle$. We take $|-3\rangle = (0, 0, -1)^T$ as the target state, which corresponds to $|\phi_0(t_f)\rangle$ for the ideal conditions $\gamma(t_f) = 0$ and $\beta(t_f) = \pi/2$. (Note that for $\epsilon \neq 0$ the initial state is not exactly $|1\rangle$. Later, in Protocol 3, we shall examine the case $|\Psi(0)\rangle = |1\rangle$.) The final fidelity with the target state is

$$F \equiv \langle -3|\Psi(t_f)\rangle = \cos \epsilon. \tag{22}$$

From Eqs. (20)–(22), we find

$$\frac{\partial \Omega_s}{\partial \epsilon} = -\frac{\pi \cos (\pi t / 2t_f)}{t_f \sin^2 \epsilon} \sim -\frac{1}{\epsilon^2}, \tag{23}$$

$$\frac{\partial \Omega_p}{\partial \epsilon} = -\frac{\pi \sin (\pi t / 2t_f)}{t_f \sin^2 \epsilon} \sim -\frac{1}{\epsilon^2}, \tag{24}$$

and

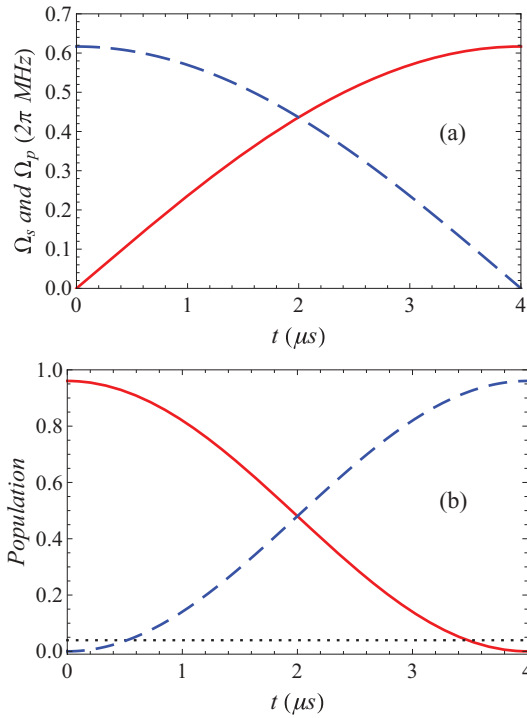$$\frac{\partial F}{\partial \epsilon} = -\sin \epsilon \sim -\epsilon, \tag{25}$$

FIG. 2. (Color online) (a) Time evolution of Rabi frequencies, $\Omega_p$ (solid red) and $\Omega_s$ (dashed blue) for $\gamma(t) = \epsilon$ and $\beta(t) = \pi t/2t_f$. (b) Time evolution of the corresponding populations of levels 1 (solid red), 2 (dotted black), and 3 (dashed blue). Parameters are as follows: $t_f = 4 \ \mu$s; $\epsilon = 0.2$.

respectively. In other words, the fidelity varies smoothly with $\epsilon$, whereas the Rabi frequencies decrease dramatically when increasing $\epsilon$. Therefore it is possible to achieve a desired fidelity with relatively small Rabi frequencies.

Improving the fidelity or shortening $t_f$ implies increasing the Rabi frequencies and the laser intensities, proportional to their squares. Note the behavior of the time-averaged frequency (interpreted geometrically as a "length" in [11]),

$$\overline{\Omega} \equiv \frac{1}{t_f} \int_0^{t_f} \sqrt{\Omega_s^2 + \Omega_p^2} \, dt = \frac{\pi \cot \epsilon}{t_f}, \qquad (26)$$

and the time-averaged energy,

$$\overline{E} \equiv \hbar \int_0^{t_f} \left( \Omega_s^2 + \Omega_p^2 \right) dt = \hbar \frac{\pi^2 \cot^2 \epsilon}{t_f}. \qquad (27)$$

*Protocol 2*. We design now a different protocol, in which the intermediate state $|2\rangle$ may be populated, and both pump and Stokes pulses vanish at $t = 0$ and $t = t_f$. Thus, we set the following boundary conditions:

$$\gamma(0) = \epsilon, \dot{\gamma}(0) = 0, \gamma(t_f) = \epsilon, \dot{\gamma}(t_f) = 0, \qquad (28)$$

$$\beta(0) = 0, \beta(t_f) = \pi/2, \qquad (29)$$

$$\gamma(t_f/2) = \delta, \dot{\beta}(0) = 0, \dot{\beta}(t_f) = 0. \qquad (30)$$

The boundary conditions in Eqs. (28) and (29) are the same as before, but we add now Eq. (30): Since the population of the intermediate state $|2\rangle$ is given by $P_2 = \sin^2 \gamma$, the
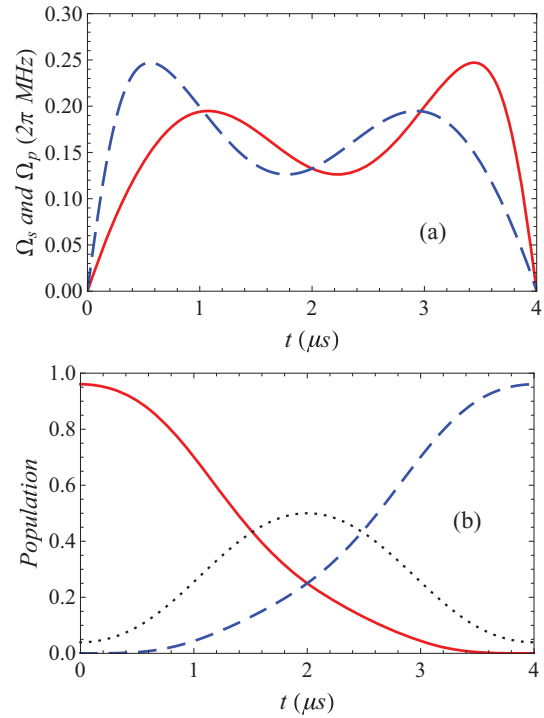


FIG. 3. (Color online) (a) Time evolution of Rabi frequencies, $\Omega_p$ (solid red) and $\Omega_s$ (dashed blue), for $\gamma(t) = \sum_{j=0}^4 a_j t^j$, and $\beta(t) = \sum_{j=0}^3 b_j t^j$, with the boundary conditions (28)–(30). (b) Time evolution of the corresponding populations of levels 1 (solid red), 2 (dotted black), and 3 (dashed blue). Parameters are as follows: $\delta = \pi/4; t_f = 4 \ \mu$s; $\epsilon = 0.2$.

condition $\gamma(t_f/2) = \delta$ sets its maximal value at $t = t_f/2$, whereas $\dot{\beta}(0) = 0$ and $\dot{\beta}(t_f) = 0$ guarantee that $\Omega_s(0) = 0$ and $\Omega_p(t_f) = 0$.

By assuming a polynomial ansatz to interpolate at intermediate times, $\gamma(t) = \sum_{j=0}^4 a_j t^j$ and $\beta(t) = \sum_{j=0}^3 b_j t^j$, we can solve the coefficients in terms of the boundary conditions. Once $\gamma(t)$ and $\beta(t)$ are fixed, we may calculate the time evolution of pulses and populations (see, e.g., Fig. 3, where $\delta = \pi/4$ is chosen as an example). Figure 3 shows that the intermediate level $|2\rangle$ is populated, and the population is 1/2 at $t = t_f/2$, because $\gamma(t_f/2) = \pi/4$. The two first protocols are compared in Figs. 2 and 3: The laser pulse intensity is smaller when the intermediate state $|2\rangle$ is allowed to be populated. Note that while sharing the SU(2) dynamical symmetry with two-level systems [18], the three-level system cannot be reduced to a two-level system.

We also calculate the time-averaged frequency and energy of Eqs. (26) and (27) in Fig. 4. They increase for a smaller $\epsilon$ as before. When $\epsilon = 0.002$ in Fig. 4, the fidelity $F = \cos \epsilon$ is equal to .999 998, which satisfies the criterion for a fault-tolerant quantum computer [5]. They also decrease significantly by populating level $|2\rangle$, though the behaviors of frequency and energy are not the same. Remarkably, Fig. 4(a) shows that the time-averaged frequency for each $\epsilon$ can be minimized. For the smallest $\epsilon$ this happens when $\delta$ approaches $\pi/2$ and the intermediate state is fully populated. The time-averaged energy is even flatter for central values of $\delta$ [see Fig. 4(b)]. When the intermediate state is not populated
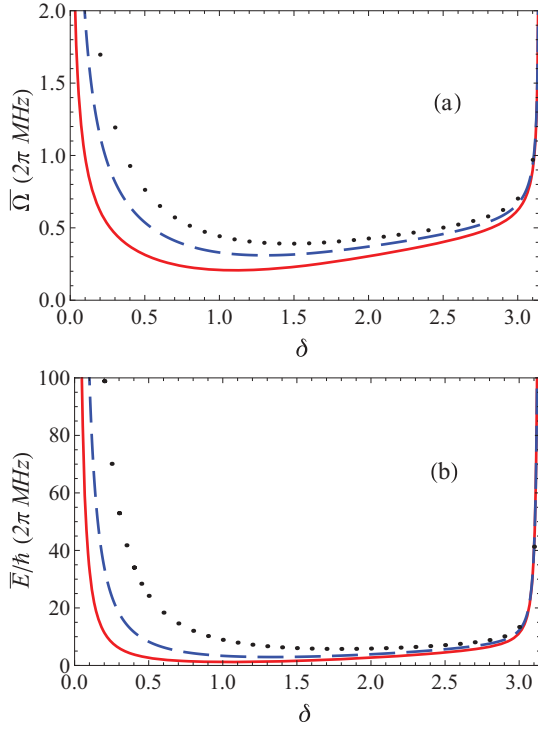
FIG. 4. (Color online) Time-averaged frequency (a) and energy (b) in the second protocol as a function of $\delta$ for different values of $\epsilon$, where $\epsilon = 0.2$ (solid red), $\epsilon = 0.02$ (dashed blue), and $\epsilon = 0.002$ (dotted black). Other parameters are the same as in Fig. 3.

at all, that is, $\delta = 0$ or $\delta = \pi$, both time-averaged energy and frequency increase dramatically.

In general we may combine the invariant-based method with optimal control to optimize the protocols according to different physical criteria [28,33,34], for example, (time-averaged) frequency minimization or energy minimization. The time-optimal problem with bounded energy, and the minimum energy cost problem for fixed time have been solved for the three-level system [11,12].

*Protocol 3.* Our last protocol is a variant of the first one, with the same pulses but a different initial state. An important difference with respect to the previous protocols is that it is based on multimode driving rather than on a single-mode driving. This means that the time-dependent wave function $|\Psi(t)\rangle$ will include contributions from the three eigenvectors of the invariant.

So far we have assumed that the initial state depends on $\epsilon$ through the dependence of $|\phi_0(0)\rangle$ on $\epsilon$. Let us instead use the bare state $|1\rangle$ as initial state but keep the designed interactions $\epsilon$ dependent as before. Figure 5 shows the fidelity $\langle -3|\Psi(t_f)\rangle$ as a function of $\epsilon$ when the initial state is $|1\rangle$. The fidelity for the $\epsilon$-dependent initial state $|\phi_0(0)\rangle$ is also shown for comparison.

Interestingly, the fidelity oscillates with respect to $\epsilon$ for the pump and Stokes pulses described by Eqs. (20) and (21). To analyze this in more detail, we first calculate the final state $\Psi(t_f) = \sum_n C_n e^{i\alpha_n} |\phi_n(t_f)\rangle$, where $C_n = \langle \phi_n(0)|1\rangle$. With the eigenvectors $|\phi_n(t)\rangle$ at $t = 0$ and $t_f$ we have

$$F \equiv \langle -3|\Psi(t_f)\rangle = e^{i\alpha_0} \cos^2 \epsilon + \frac{1}{2}(e^{i\alpha_+} + e^{i\alpha_-}) \sin^2 \epsilon. \quad (31)$$
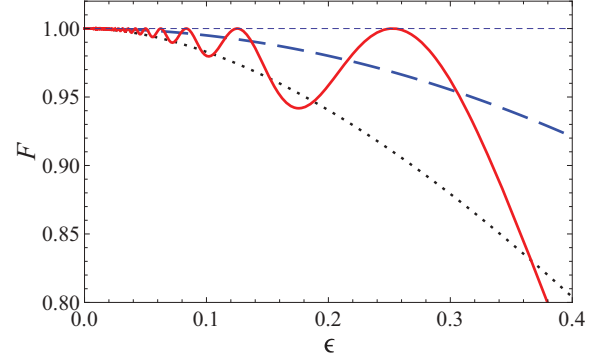


FIG. 5. (Color online) Fidelity versus $\epsilon$ for the initial state $|1\rangle$: solid red and dotted black lines correspond to the examples 1 and 2 in Figs. 2 and 3. The fidelity $F = \cos \epsilon$ (dashed blue) for the initial state $|\phi_0(0)\rangle$ is also shown.

The Lewis-Riesenfeld phases $\alpha_n$ are

$$\alpha_0 = 0, \alpha_\pm = \mp \frac{\pi}{2 \sin \epsilon}, \quad (32)$$

which finally gives

$$F = 1 - \sin^2 \epsilon \left\{ 1 - \cos \left( \frac{\pi}{2 \sin \epsilon} \right) \right\}. \quad (33)$$

When the condition

$$(\sin \epsilon)^{-1} = 4N, (N = 1, 2, 3...) \quad (34)$$

is satisfied, the fidelity becomes 1. By solving Eq. (34), we get $\epsilon = 0.2527$ for $N = 1$, $\epsilon = 0.1253$ for $N = 2$, etc. In particular, the rightmost maximum at $\epsilon = 0.2527$ combined with the initial state $|1\rangle$ provides perfect population transfer, as shown in Fig. 6, with less intensities than the ones required in the first protocol for a good fidelity, since the value of $\epsilon$ is relatively large now. Compare the values $\overline{\Omega} = 2\pi \times 0.48$ MHz and $\overline{E}/\hbar = 2\pi \times 5.89$ MHz for $\epsilon = 0.2527$ in Protocol 3 (with fidelity $F = 1$) by using Eqs. (26) and (27), with $\overline{\Omega} = 2\pi \times 0.62$ MHz and $\overline{E}/\hbar = 2\pi \times 9.56$ MHz for $\epsilon = 0.2$ (corresponding to $F = 0.9682$) in the first protocol. To achieve higher fidelity in the first protocol, for example, $F = 0.9998$, the time-averaged frequency and energy have to be increased
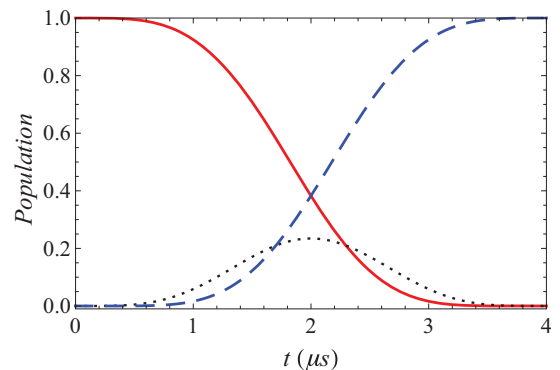


FIG. 6. (Color online) Time evolution of the populations of levels 1 (solid red), 2 (dotted black), and 3 (dashed blue), where the pump and Stokes pulses are described by Eqs. (20) and (21), and the initial state is $|1\rangle$. Parameters are as follows: $t_f = 4 \mu s$; $\epsilon = 0.2527$.

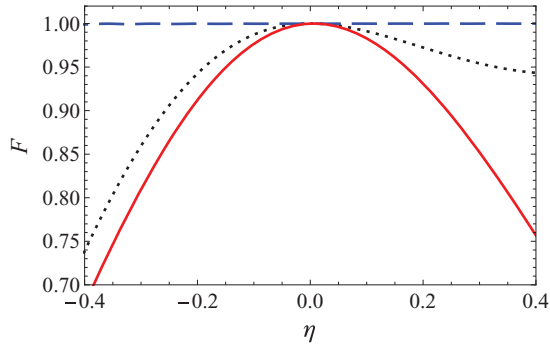FIG. 7. (Color online) Fidelity versus the change of pump and Stokes pulses from $\Omega_s$ and $\Omega_p$ to $\Omega_s(1 + \eta)$ and $\Omega_p(1 + \eta)$. Protocol 1 (dashed blue) with $\epsilon = 0.02$, Protocol 2 (dotted black) with $\epsilon = 0.02$ and $\delta = \pi/4$, and Protocol 3 (solid red) with $\epsilon = 0.2527$. The initial state is $|1\rangle$ and $t_f = 4\,\mu$s.

up to $\overline{\Omega} = 2\pi \times 6.25$ MHz and $\overline{E}/\hbar = 2\pi \times 981.49$ MHz by choosing $\epsilon = 0.02$. In summary, Protocol 3, based on multimode driving, provides an alternative shortcut to implement a perfect population transfer with a low energy cost.

To check the stability, we compare the fidelity versus systematic errors for different Protocols 1, 2 and 3. Protocol 3, which makes use of multimode interference as in $\pi$ pulses for two-level systems, turns out to be more sensitive to the systematic errors than the other protocols (see Fig. 7), but the smaller laser intensities make it more robust with respect to amplitude noise. Different stability properties may be in general expected with respect to different perturbations [22], and further work is necessary to optimize the inverse-engineered protocols with respect to several experimental conditions.

## IV. DISCUSSIONS AND CONCLUSIONS

In this paper we have applied and developed the invariant-based inverse engineering method to achieve fast population transfers in a three-level system. Two different single-mode protocols are applied first in which the fidelity is linked to the laser intensity. Shortening the time also implies an energy cost. To achieve the same fidelity, less intensity is required when the intermediate level $|2\rangle$ is populated. The population of the intermediate level is usually problematic when its time decay scale is smaller than the process time. While this may be a serious drawback for an adiabatic slow process, it need not be for a fast shortcut. Protocols that populate level 2 may

thus be considered as useful alternatives for certain systems and sufficiently short process times.

A variant of the first protocol in which the initial state is simply the bare state $|1\rangle$ and the dynamics is driven by a multimode wave function provides a less costly shortcut. Further exploration of the multimode approach in this and other systems is left for a separate study.

As we stated in the introduction, different techniques to find shortcuts to adiabaticity are strongly related, or even equivalent. The invariant-based inverse method presented here may be compared to the optimal control approaches in Refs. [9–11]. Invariant-based inverse engineering provides a complementary perspective of these approaches, whereas optimal control is useful to choose among the possible solutions found by the invariant-based inverse engineering. In the optimal control method used in Ref. [11], the system of control differential equations coincides with Eqs. (7) and (8) in the invariant method. The ultimate reason is that these equations are in fact equivalent to the Schrödinger equation for a given wave-function parametrization. The optimal protocol in Ref. [11] corresponds to single-mode driving: The solution of the dynamics is assumed to be the eigenstate of invariant $|\phi_0(t)\rangle$. Multimode driving is allowed in the optimal control method applied in Refs. [9,10]. The optimal functions for the pump and Stokes pulses which maximize the unconstrained cost functional $J = \langle -3|\Psi(t_f)\rangle + \lambda \int_0^{t_f} dt(\Omega_s^2 + \Omega_p^2)$, where $\lambda$ is some weight, have the functional structure used in Protocol 3, but note that the fidelity in Protocol 3 is one by construction.

Finally, the present results——within the on-resonance condition—are applicable to quantum state transfer with three qubits [42], adiabatic splitting or transport of atoms in a double well, and a triple well [43]. In a more general case, the Hamiltonian (1) ($\Delta_p \neq 0$ and $\Delta_3 \neq 0$) does not possess SU(2) symmetry, so that the invariant $I(t)$ should be constructed in terms of the eight Gell-Mann matrices for the SU(3) group [44]. The invariant-based inverse engineering for the three-level systems with Gell-Mann dynamic symmetry and the extension to N-level systems with SU(2) or SU(3) dynamic symmetry [45,46] will be discussed elsewhere.

[1] L. Allen and J. H. Eberly, *Optical Resonance and Two-level Atoms* (Dover, New York, 1987).

[2] K. Bergmann, H. Theuer, and B. W. Shore, Rev. Mod. Phys. **70**, 1003 (1998).

[3] N. V. Vitanov, T. Halfmann, B. W. Shore, and K. Bergmann, Annu. Rev. Phys. Chem. **52**, 763 (2001).

[4] P. Král, I. Thanopulos, and M. Shapiro, Rev. Mod. Phys. **79**, 53 (2007).

[5] M. Saffman, T. G. Walker, and K. Mølmer, Rev. Mod. Phys. **82**, 2313 (2010).

[6] M. Levitt, Prog. Nucl. Magn. Reson. Spectrosc. **18**, 61 (1986).

[7] B. T. Torosov and N. V. Vitanov, Phys. Rev. A **83**, 053420 (2011).

[8] B. T. Torosov, S. Guérin, and N. V. Vitanov, Phys. Rev. Lett. **106**, 233001 (2011).

[9] V. S. Malinovsky and D. J. Tannor, Phys. Rev. A **56**, 4929 (1997).

[10] I. R. Solá, V. S. Malinovsky, and D. J. Tannor, Phys. Rev. A **60**, 3081 (1999).

[11] U. Boscain, G. Charlot, J.-P. Gauthier, S. Guérin, and H.-R. Jauslin, J. Math. Phys. **43**, 2107 (2002).

[12] D. Sugny and C. Kontz, Phys. Rev. A **77**, 063420 (2008).

[13] G. S. Vasilev, A. Kuhn, and N. V. Vitanov, Phys. Rev. A **80**, 013417 (2009).

[14] M. Demirplak and S. A. Rice, J. Phys. Chem. A **107**, 9937 (2003); J. Phys. Chem. B **109**, 6838 (2005); J. Chem. Phys. **129**, 154111 (2008).

[15] M. V. Berry, J. Phys. A **42**, 365303 (2009).

[16] X. Chen, I. Lizuain, A. Ruschhaupt, D. Guéry-Odelin, and J. G. Muga, Phys. Rev. Lett. **105**, 123003 (2010).

[17] M. G. Bason, M. Viteau, N. Malossi, P. Huillery, E. Arimondo, D. Ciampini, R. Fazio, V. Giovannetti, R. Mannella, and O. Morsch, Nat. Phys. **8**, 147 (2012).

[18] X. Chen, E. Torrontegui, and J. G. Muga, Phys. Rev. A **83**, 062116 (2011).

[19] S. Ibáñez, S. Martínez-Garaot, X. Chen, E. Torrontegui, and J. G. Muga, Phys. Rev. A **84**, 023415 (2011).

[20] M.-A. Fasihi, Y.-D. Wan, and M. Nakahara, J. Phys. Soc. Jpn. **81**, 024007 (2012).

[21] S. Ibáñez, X. Chen, E. Torrontegui, A. Ruschhaupt, and J. G. Muga, arXiv:1112.5522.

[22] A. Ruschhaupt, X. Chen, D. Alonso, and J. G. Muga, arXiv:1206.1691.

[23] S. Masuda and K. Nakamura, Proc. R. Soc. A **466**, 1135 (2010); Phys. Rev. A **84**, 043434 (2011).

[24] J. G. Muga, X. Chen, A. Ruschhaup, and D. Guéry-Odelin, J. Phys. B **42**, 241001 (2009).

[25] X. Chen, A. Ruschhaupt, S. Schmidt, A. del Campo, D. Guéry-Odelin, and J. G. Muga, Phys. Rev. Lett. **104**, 063002 (2010).

[26] E. Torrontegui, S. Martínez-Garaot, A. Ruschhaupt, and J. G. Muga, Phys. Rev. A **86**, 013601 (2012).

[27] X. Chen and J. G. Muga, Phys. Rev. A **82**, 053403 (2010).

[28] D. Stefanatos, J. Ruths, and J. S. Li, Phys. Rev. A **82**, 063422 (2010).

[29] J. F. Schaff, X.-L. Song, P. Vignolo, and G. Labeyrie, Phys. Rev. A **82**, 033430 (2010).

[30] J. F. Schaff, X. L. Song, P. Capuzzi, P. Vignolo, and G. Labeyrie, Europhys. Lett. **93**, 23001 (2011).

[31] J. F. Schaff, P. Capuzzi, G. Labeyrie, and P. Vignolo, New J. Phys. **13**, 113017 (2011).

[32] E. Torrontegui, S. Ibáñez, X. Chen, A. Ruschhaupt, D. Guéry-Odelin, and J. G. Muga, Phys. Rev. A **83**, 013415 (2011).

[33] X. Chen, E. Torrontegui, D. Stefanatos, J.-S. Li, and J. G. Muga, Phys. Rev. A **84**, 043415 (2011).

[34] E. Torrontegui, X. Chen, M. Modugno, S. Schmidt, A. Ruschhaupt, and J. G. Muga, New J. Phys. **14**, 013031 (2012).

[35] Y. Li, L.-A. Wu, and Z.-D. Wang, Phys. Rev. A **83**, 043804 (2011).

[36] A. del Campo, Phys. Rev. A **84**, 031606(R) (2011); Europhys. Lett. **96**, 60005 (2011).

[37] S. Choi, R. Onofrio, and B. Sundaram, Phys. Rev. A **84**, 051601(R) (2011).

[38] R. G. Unanyan, L. P. Yatsenko, K. Bergmann, and B. W. Shore, Opt. Commun. **139**, 48 (1997).

[39] C. E. Carroll and F. T. Hioe, J. Opt. Soc. Am. B **5**, 1335 (1988).

[40] Y.-Z. Lai, J.-Q. Liang, H. J. W. Müller-Kirsten, and J.-G. Zhou, Phys. Rev. A **53**, 3691 (1996); J. Phys. A **29**, 1773 (1996).

[41] H. R. Lewis and W. B. Riesenfeld, J. Math. Phys. **10**, 1458 (1969).

[42] S.-C. Oh, Y.-P. Shim, J.-J. Fei, M. Friesen, and X.-D. Hu, arXiv:1201.4829.

[43] Y. Loiko, V. Ahufinger, R. Corbalán, G. Birkl, and J. Mompart, Phys. Rev. A **83**, 033629 (2011).

[44] F. T. Hioe, Phys. Rev. A **32**, 2824 (1985).

[45] F. T. Hioe and J. H. Eberly, Phys. Rev. Lett. **47**, 838 (1981).

[46] F. T. Hioe, J. Opt. Soc. Am. B **4**, 1327 (1987); **5**, 859 (1988).